Acoustic wave propagation in heterogeneous two-dimensional fractured porous media

Hossein Hamzehpour,[1,2,*] Mojgan Asgari,[1] and Muhammad Sahimi[3]
[1]*Department of Physics, K. N. Toosi University of Technology, Tehran 15875-4416, Iran*
[2]*School of Physics, Institute for Research in Fundamental Sciences (IPM), Tehran 19395-5531, Iran*
[3]*Mork Family Department of Chemical Engineering and Materials Science, University of Southern California, Los Angeles, California 90089-1211, USA*
(Received 21 October 2015; revised manuscript received 11 April 2016; published 13 June 2016)

This paper addresses an important fundamental question: the differences between wave propagation in fractured porous media with a uniform matrix (constant bulk modulus) and those in which the matrix is heterogeneous with its bulk modulus distributed spatially. The analysis of extensive experimental data [Phys. Rev. E **71**, 046301 (2005)] indicated that such distributions are self-affine and induce correlations at all the relevant length scales. The comparison is important from a practical view point because in many of the traditional models of fractured rock, particularly those that are used to study wave propagation or fit some data, the matrix is assumed to be uniform. Using extensive numerical simulation of propagation of acoustic waves, we present strong evidence indicating that the waves' amplitude in a fractured porous medium with a heterogeneous matrix decays exponentially with the distance from the source. This is in sharp contrast with a fractured porous medium with a uniform matrix in which not only the waves' amplitude decays with the distance as a *stretched* exponential function, but the exponent that characterizes the function is also dependent upon the fracture density. The localization length depends on the correlations in the spatial distribution of the bulk modulus, as well as the fracture density. The mean speed of the waves varies linearly with the fractures' mean orientation.

DOI: 10.1103/PhysRevE.93.063305

I. INTRODUCTION

Two important characteristics of many field-scale (FS) porous media, such as groundwater aquifers and oil, gas, and geothermal reservoirs, are their broad heterogeneity and fracture network. The heterogeneities of such formations are manifested by broad spatial distributions of the porosity, permeability, and elastic moduli [1–3]. Three decades ago Hewett [4] presented strong evidence that the porosity logs of the FS porous media in the direction perpendicular to the bedding follows the statistics of a fractional Gaussian noise (FGN) [5], while those parallel to the bedding follow a fractional Brownian motion (FBM) [4], where the former is the "numerical derivative" of the latter. Both the FGN and FBM are self-affine stochastic functions that induce correlations with an infinite correlation length. As FS porous media have a finite size, an infinite correlation length implies one whose extent is as large as the linear size of the media under study. Numerous studies over the past three decades have shown that the permeability [6,7] and elastic moduli [8] of FS porous media also follow such self-affine distributions. For a comprehensive review see Ref. [2]. Thus, any realistic modeling of an FS porous medium must take into account the effect of such long-range correlations in their various properties.

Many FS porous media are also highly fractured [1–3,9–11]. Fractures are crucial to flow of fluids in FS porous media and act as fast conduits for dispersal of contaminants in low-permeability soils [12], and their spatial distribution is critical to understanding tectonic motions [13–15]. They also provide important clues to the spatial distribution of earthquake hypocenters [16–19]. Thus, comprehensive characterization and modeling of FS porous media entails taking into account the effect of the heterogeneities and their extended correlations, as well as the spatial distribution of the fractures.

An important impediment to characterization of FS porous media and, hence, their modeling is the difficulty of measuring and collecting data for their properties. One method for collecting such data is through well bores. During drilling of wells in FS porous media, many properties are measured at various depths [20–22] and recorded. These are usually referred to as well logs. It was through the analysis of such well logs that their aforementioned self-affine structure was discovered. Such logs include porosity, resistivity, gamma ray, sonic transient times, and other information.

Another method for gaining information and insight into the structure of FS porous media is seismic experiments. An explosion is carried out on the surface. The resulting seismic waves, representing waves of energy, propagate throughout the formation and are reflected by the body of the porous formation. The reflections carry information on the spatially varying heterogeneities of the formation. By recording the reflections and the differences in the arrival times of the primary and secondary (P and S, respectively) waves and other characteristics, one gains information about the structure of porous formations.

The general problem propagation of waves in heterogeneous porous materials and media is of interest not only to petroleum engineering but also to a wide variety of other science and engineering disciplines, including geophysics, soil science, oceanography, and characterization and modeling of FS porous media. In particular, propagation and reflection of seismic waves are used [23,24] to estimate not only the hydrocarbon content of a potential oil reservoir, but also the spatial distributions of its strata and fractures. Although seismic records do not have high resolution and cannot provide meaningful information on length scales smaller than 9–15 meter, they provide a relatively accurate picture of the large-scale structure of FS porous media.

*hamzehpour@kntu.ac.ir

In a series of papers we studied wave propagation in highly heterogeneous media. Both acoustic [25,26] and elastic [27,28] waves were considered, and it was assumed, in accordance with the analysis of well logs for the same properties [8], that the elastic constants of the media follow an FBM. One important goal of the study was whether such waves are localized in heterogeneous porous media, similar to the classical problem of electron localization in disordered solids. We found that both acoustic and elastic waves are localized in two-dimensional (2D) heterogeneous porous media. In particular, due to localization, the wave front in 2D porous media in which the elastic constants follow an FBM distribution takes on [29] the shape of the rough landscape generated by the 2D FBM, with its roughness exponent being equal to the Hurst exponent H that characterizes the FBM. Although the one-loop dynamic renormalization group approach that we utilized in our theoretical studies [25–28] indicated that both acoustic and elastic waves are also localized in 3D porous media, if the distribution of their elastic constants follows an FBM, numerical simulation of the phenomena has not provided an unambiguous resolution of the problem.

The question of wave localization in the FS porous media is particularly important from a practical point of view. If the waves are localized, then any information that their scattering conveys over length scales that are larger than the localization correlation length is useless and represents only statistical noise due to the heterogeneity of the porous formations. The localization correlation length depends, of course, on the structure of porous media and the spatial distribution of their heterogeneities.

In a recent paper [30] we studied propagation of acoustic waves in a model fractured porous medium. Unlike most of the models of fractures used in the past in which no finite thickness was attributed to them, we represented, following Yazdi *et al.* [31] (see also Refs. [32–34]), the fractures by channels of finite lengths and thicknesses; the authors of Ref. [31] presented strong numerical evidence that the finite thickness of the fractures has a strong influence on the connectivity and flow and transport properties of a fractured porous medium. In particular, it gives rise to nonuniversal power laws for the various properties of the system near its connectivity or percolation threshold. In our study of propagation of acoustic waves [30] the matrix was assumed to be uniform, but with constant elastic constants. We found that the amplitude A of the waves decays as

$$A \propto \exp[-\gamma(\rho,b)x^{\alpha}]. \tag{1}$$

Here b is the fractures' thickness, ρ is their density (volume fraction), γ a coefficient with units of $1/(length)^{\alpha}$, and x the distance from the waves' source. The most interesting aspect of this result was that, at large distances x from the wave source, the exponent α is not only strictly less than 1, but also depends on both ρ and b. This is an unexpected result in that it implies that the presence of fractures of finite length and thickness *slows down* the decay of the waves' amplitude. It is also unlike the classical electron localization in disordered solids in which the amplitude decays exponentially fast, i.e., $\alpha = 1$.

Thus, the focus of this paper is on the propagation of acoustic waves in the same type of model of fractured porous media, but those in which the matrix is no longer uniform. Instead, the bulk modulus of the matrix is, in accordance with the well logs for the elastic properties of rock [8], distributed according to an FBM. In our opinion, this would make the model of fractured porous media that we develop a realistic model, close to what field observations [2] and well logs [8,20–22] suggest. We address a fundamental question: Is the decay of the waves' amplitude still a stretched exponential function, or is it faster and similar to the classical electron localization? From a practical point of view, the question is important. If the waves' amplitude in fractured porous media decays slower than exponentially, the implication is that such techniques as seismic wave propagation provide more information about the structure of such porous media than unfractured media. In an interesting study Garnier and Sølna [35] explained the relation between the effective attenuation and dispersion of an acoustic wave propagation through a random medium on the medium's statistics, such as its short- or long-range correlation properties.

But, in addition to the fundamental problem of wave localization, propagation of acoustic waves in porous media is also of interest because of its many practical applications. Stimulation of oil reservoirs by weak elastic waves was a technique that was used from the 1950s to 1970s [36,37]. The interest has been revived over the past decade by the observations that oil fields that are close to regions with earthquakes, or even those with heavy traffic, produce more. Thus, the idea of using waves to stimulate oil reservoirs has been resurgent. Two types of waves have been used [38]. One consists of high-power frequency waves that affect a reservoir locally and are used for *well stimulation*. The second type consists of low-frequency acoustic waves [38] that stimulate an entire reservoir.

Another application of acoustic wave propagation in porous media is to measurement of the velocity and density of the fluids in porous formations using various techniques, such as a double-pulse signal emitted from an ultrasonic transducer [39]. A third application is using acoustic waves in wireless data telemetry in oil well services. The method [40] utilizes compressional acoustic waves to transmit data along the drill string. To do so, coded wave trains are produced by an acoustic transducer that travel through the drill string. They are subsequently decoded to recover the data. Clearly the travel time of the coded wave trains depends on the structure of rock and in particular its heterogeneity. Sonic well logging, which is based on propagation of acoustic waves, is used for borehole measurements, such as estimating the porosity of a porous formation [41]. It is also used for detecting fractures [42,43] that intersect the well along which logging is run.

The P and S waves in a fractured porous medium interact and mix. Thus, a study of such waves and their speed must in principle involve the solution of the elastic wave equation. However, studying this aspect is not our goal in this paper. Rather, we are interested in the localization properties of the waves and their dependence on the structure of fractured porous media. At the same time, due to its many aforementioned applications, as well as the fundamental problem of wave localization, study of propagation of acoustic waves in fractured porous media is an important and interesting problem on its own merit. Moreover, if we view the fractures

as high-conductivity zones in a disordered medium, then our study also represents an attempt for understanding propagation and localization of acoustic waves in a highly heterogeneous solid, which is also a problem of much interest.

Before presenting the details of the work, it would be instructive to review the previous works and their differences with what we study in this paper. Saenger *et al.* [44] introduced a numerical scheme based on a rotated staggered computational grid to solve the wave equation but did not study fractured porous media. Saenger and Shapiro [45] studied wave propagation in a porous medium with thin intersecting cracks. However, no finite dimension was attributed to the cracks, and the crack density was low, significantly below the percolation threshold. As our recent paper demonstrated [30], a finite dimension of the cracks gives rise to nonuniversality and unexpected results for flow and transport properties of fractured porous media and fracture networks and, thus, cannot be ignored. Saenger *et al.* [46] studied wave propagation in 3D porous media with nonintersecting thin penny-shape cracks in three dimensions that do not form a sample-spanning percolation cluster. The critical crack density or percolation threshold of the system that they studied is between ≈ 0.18 [47] and ≈ 0.23 [1]. Both papers [45,46] were also concerned only with wave velocities and testing the accuracy of the effective-medium approximation of O'Connell and Budiansky [48].

Orlowsky *et al.* [49] simulated wave propagation in 2D porous media with thin (zero cross-sectional area) parallel fractures, which is not relevant to our study. Vlastos *et al.* [50] studied wave propagation in a porous medium with short, nonintersecting, thin (zero cross section) cracks that were more or less parallel. In another study Vlastos *et al.* [51] investigated the effect of pore pressure and carried out dual fluid flow and wave propagation simulations, which were not, however, coupled due to the differences in the time scales involved in wave propagation and fluid flow. In their model the main fractures were parallel and generated by a cellular automata model [52]. Hall and Wang [53] studied wave propagation in fractured porous media using an equivalent medium in which the elastic coefficients were averaged over a fractured space. The fractures were, however, parallel and nonintersecting.

Therefore, although a considerable amount of work has been carried out on simulation of wave propagation in fractured porous media, the models used in almost all cases were far simpler and in our opinion less realistic than what we utilized in the present paper. In addition, these works assumed that the porous medium matrix is uniform, whereas a major goal of the present paper is to study the effect of the heterogeneity in the porous matrix on wave propagation.

The organization of this paper is as follows. In Sec. II we describe the model of fractured porous media that we use in our study. Section III presents the governing equations for acoustic wave propagation, and the numerical technique for solving the governing equation is described in Sec. IV. The results are presented and discussed in Sec. V. The paper is summarized in Sec. VI.

II. MODEL OF FRACTURED POROUS MEDIUM

Although the model that we utilize in this paper was previously described in Refs. [30–33], for the sake of completeness we describe briefly its essential features. A 2D model is utilized, represented by a square grid of size $L_x \times L_y$, with $L_x = N_x a$ and $L_y = N_y a$, where a is the size of the elementary square block in the grid, and $N_x = 4096$ and $N_y = 512$ in all of our simulations.

The matrix of the porous media is not uniform. Each grid block is characterized by an elastic constant (bulk modulus), selected from an FBM array. To generate the spatial distribution of the bulk modulus of the grid blocks according to an FBM, we used the fast Fourier transformation method. The spectral density $S(\boldsymbol{\omega})$ of a d- dimensional FBM, the Fourier transform of its covariance, is given by

$$S(\boldsymbol{\omega}) = \frac{a(d)}{\left(\sum_{i=1}^{d} \omega_i^2\right)^{H+d/2}}, \tag{2}$$

where, $\boldsymbol{\omega} = (\omega_1, \ldots, \omega_d)$ is the Fourier transform variable and $a(d)$ is a d- dependent constant. Here H is the Hurst exponent that controls the type of correlation. $H > 1/2 (H < 1/2)$ indicates positive (negative) correlations in the successive increments of the FBM, and $H = 1/2$ represents the Brownian (completely random) case with no correlations between the increments. Thus, in accordance with the analysis of extensive data for the elastic properties and wave speeds of FS porous media [8], we generated 2D FBM arrays of size 4096×512 and attributed the results to the blocks of the computational grid as their elastic constant.

The fractures are represented by rectangles of length l and width b. The location of the fractures' center and their orientation were both assumed to follow uniform distributions, although it would impose no additional difficulty to use other types of distributions. The width and length of the fractures are $2a$ and $64a$, respectively. Accordingly, the fracture number density ρ is given by $\rho = N_f/(L_x \times L_y)$, where N_f is the number of fractures. Periodic boundary conditions in both horizontal and vertical directions were used to generate the fracture network. The network is embedded in the porous matrix and surrounded by grid blocks whose elastic constant follows an FBM, as described earlier. Two samples of the generated fractured porous medium are shown in Fig. 1 for which the Hurst exponent is $H = 0.5$. Figure 2 presents a sample of the fractured porous medium with a distribution of the bulk modulus of the grid blocks in the matrix that follow an FBM with $H = 0.2$.

III. GOVERNING EQUATION

Propagation of acoustic waves is described by the scalar wave equation [23,54]

$$\rho_m(\mathbf{x}) \frac{\partial^2}{\partial t^2} \psi(\mathbf{x},t) = \nabla \cdot [K(\mathbf{x}) \nabla \psi(\mathbf{x},t)] + S(t), \tag{3}$$

where $K(\mathbf{x})$ and $\rho_m(\mathbf{x})$ are, respectively, the bulk modulus and density of the medium at point $\mathbf{x}$, and $S(t)$ is the strength of the source, which in our simulation is placed at the "top" of the medium; see Fig. 1. In Eq. (3) $\psi(\mathbf{x},t)$ represents the amplitude of the wave at position $\mathbf{x}$ and time t. In 2D media that we study Eq. (3) describes the transverse displacement in the system with varying tension and mass density, or antiplane shear in a 2D heterogeneous solid [55]. In strongly heterogeneous media, both $K(\mathbf{x})$ and $\rho_m(\mathbf{x})$ vary spatially. In our simulation

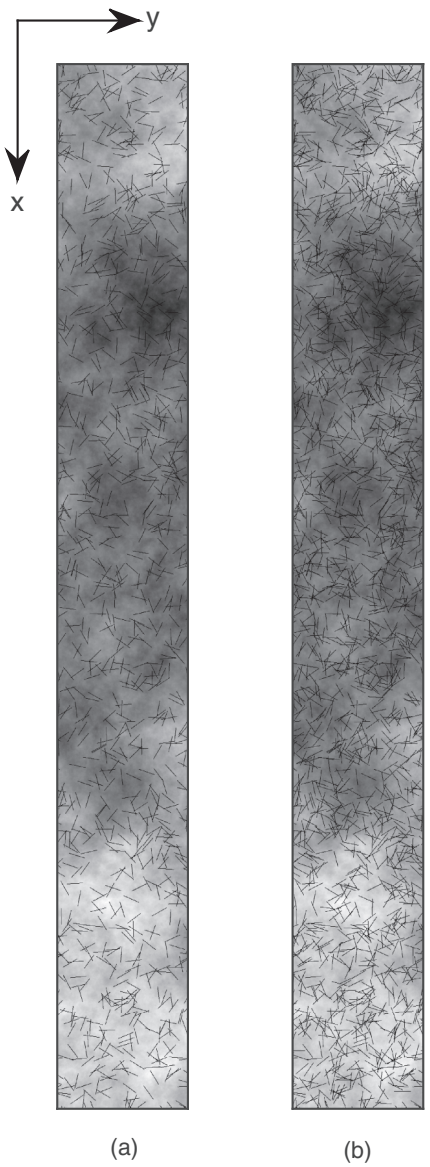

FIG. 1. Distribution of the bulk modulus of fractured porous media with $H = 0.5$ and for (a) fracture density $\rho = 2$ and (b) $\rho = 4$. The fractures' length is $l = 64a$ and their width is $b = 2a$. The medium's size is $L_x = 4096a$ and $L_y = 512a$. x is the main direction of wave propagation. Lighter colors indicate larger bulk modulus.

the bulk modulus of the grid blocks representing the matrix is distributed spatially according to a FBM, as described earlier. The mass density of the porous matrix and the fractures were taken to be 1 and 0.7, respectively. These are the typical values that have been used in the past.

IV. NUMERICAL SIMULATION

Using the length l of the fractures as a basic length scale, we first rescale the variables,

$$x' = \frac{x}{l}, \quad L'_x = \frac{L_x}{l}, \quad L'_y = \frac{L_y}{l}, \quad b' = \frac{b}{l}, \quad \rho' = \rho l^2, \quad (4)$$

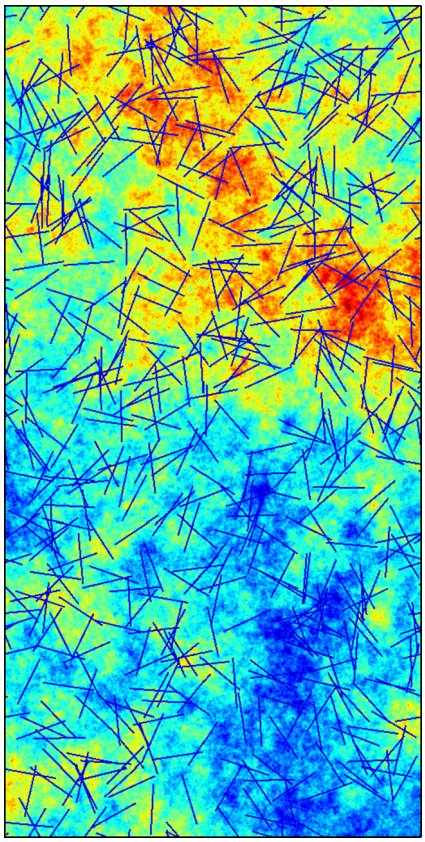

FIG. 2. Distribution of the bulk modulus of a fractured porous medium with a Hurst exponent $H = 0.2$. The medium's size is $L_x = 1024a$ and $L_y = 512a$. x is the main direction of wave propagation. Shades of red indicate larger bulk modulus.

and for convenience drop the prime notation. To solve Eq. (3) numerically, we use the finite-difference (FD) method with second-order discretization for the time and fourth-order discretization for the spatial variables, in order to avoid numerical dispersion. The standard form of the second-order FD approximation (accurate to Δt^2) is given by

$$\frac{\partial^2 \psi(\mathbf{x},t)}{\partial t^2} \simeq \frac{\psi_{i,j}^{(n+1)} - 2\psi_{i,j}^{(n)} + \psi_{i,j}^{(n-1)}}{\Delta t^2}, \quad (5)$$

where Δt is the size of the time step, taken for all the cases to be $\Delta t = 10^{-2}$, and the superscripts denote the time step numbers. As for the spatial derivatives, we first expand the right side of Eq. (3):

$$\begin{aligned}\nabla \cdot [K(\mathbf{x})\nabla\psi(\mathbf{x},t)] &= \nabla K(\mathbf{x}) \cdot \nabla\psi(\mathbf{x},t) + K(\mathbf{x})\nabla^2\psi(\mathbf{x},t) \\ &= \partial_x K(\mathbf{x})\partial_x\psi(\mathbf{x},t) + \partial_y K(\mathbf{x})\partial_y\psi(\mathbf{x},\mathbf{t}) \\ &\quad + K(\mathbf{x})\left[\partial_x^2\psi(\mathbf{x},t) + \partial_y^2\psi(\mathbf{x},t)\right],\end{aligned}$$

and then use the fourth-order FD discretization to obtain, for example, for the derivatives in the x direction

$$\partial_x^2\psi(\mathbf{x},t) \simeq \frac{-\psi_{i+2,j}^{(n)} + 16\psi_{i+1,j}^{(n)} - 30\psi_{i,j}^{(n)} + 16\psi_{i-1,j}^{(n)} - \psi_{i-2,j}^{(n)}}{12\Delta x^2} \quad (6)$$

and

$$\partial_x \psi(\mathbf{x},t) \simeq \frac{-\psi^{(n)}_{i+2,j} + 8\psi^{(n)}_{i+1,j} - 8\psi^{(n)}_{i-1,j} + \psi^{(n)}_{i-2,j}}{12\Delta x}, \quad (7)$$

where Δx is the spacing between two neighboring grid points in the x direction. The accuracy of such approximations and numerical stability of the method [56,57] were verified by preliminary simulations in the limit of low frequencies or wavelengths that are much larger than the linear size of the blocks of the computational grid. We took $\Delta x = \Delta y = a$, with the main direction of wave propagation being the x direction; see Fig. 2. To avoid the boundary effects we used periodic boundary condition in y direction. The discretized form of Eq. (3) was solved with up to 44 000 time steps.

The wave source was put at every node of the grid's first row at $x = 0$ (Fig. 1), ensuring generation of a smooth initial wave front. The source function $S(t)$ that we used was the pulse wave,

$$S(t) = A \ \exp[-\zeta(t - t_0)^2], \quad (8)$$

where we assume $A = 1$ at the source points; $t_0 = 10^5 \Delta t$, and $\zeta = 5 \times 10^{-5}$ control the waves' wavelength and their width. The receivers (grid points) at which the data are collected and analyzed are distributed evenly throughout the grid along the main direction of wave propagation. The energy of a propagating wave is given by [55]

$$E_P = \frac{1}{2}\rho_m(\mathbf{x})\left[\frac{\partial\psi(\mathbf{x},t)}{\partial t}\right]^2 + \frac{1}{2}K(\mathbf{x})[\nabla\psi(\mathbf{x},t)]^2. \quad (9)$$

V. RESULTS AND DISCUSSION

We studied several characteristics of the propagating waves in the model heterogeneous fractured porous medium described earlier. In what follows we present and discuss the results.

A. Decay of the waves' amplitude

Figure 3 presents the decay of the amplitude A as a function of the distance x from the source, fracture number densities ρ, and the Hurst exponents H, for a constant fracture width, $b = 0.0313$. It is clear that the waves' amplitude decays rapidly with x and follows an equation similar to Eq. (1), except that the coefficient γ depends on ρ and the Hurst exponent H:

$$A \propto \exp[-\gamma(\rho,H)x^{\alpha}]. \quad (10)$$

Moreover, at a fixed distance x from the source and fixed Hurst exponent H, A decreases very rapidly with increasing fracture number density ρ. There is also a qualitative difference between $H < 0.5$ and $H > 0.5$. Figure 3 indicates that the rate of decay of the wave amplitude for $H < 0.5$ is larger than those for $H > 0.5$. The reason is the nature of the correlations: $H < 0.5$ corresponds to negative correlations, large values of the bulk modulus of grid blocks next to small values, and hence a more heterogeneous medium that causes a more rapid decay of the amplitudes.

We find that, $\alpha \approx 1$, independent of H and ρ. As discussed in the introduction, in the case of a uniform matrix with constant bulk modulus [30], we found that $\alpha < 1$ and that α is a function of the fracture density and width. The coefficient

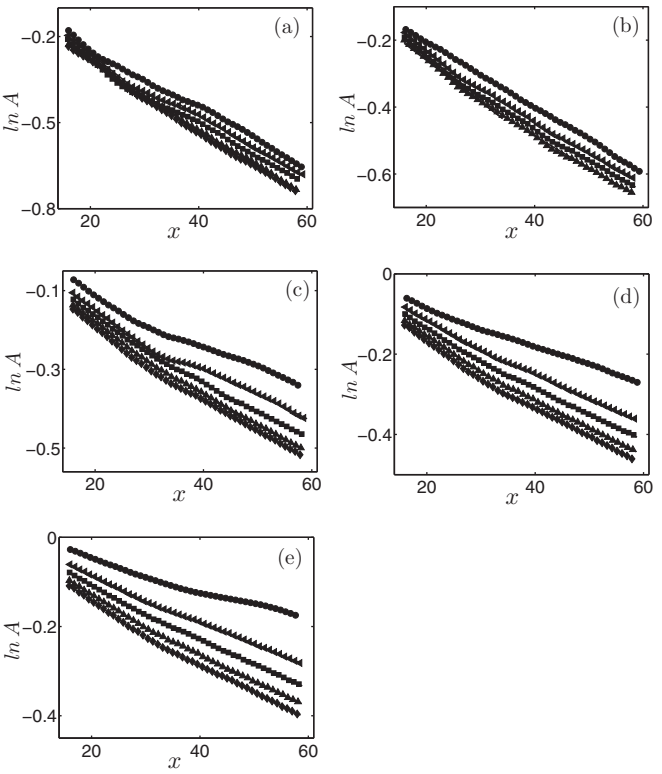

FIG. 3. Decay of the wave amplitude A versus the distance x from the source for the Hurst exponents (a) $H = 0.25$, (b) 0.3, (c) 0.5, (d) 0.6, and (e) 0.75. The results are for fracture density $\rho = 0$ (●), 1 (◀), 2 (■), 3 (▲), and 4 (♦).

γ depends on ρ and H. For short distances x from the source shown in Fig. 2, γ varies with ρ and H as presented in Fig. 4. A power law fits the numerical data well:

$$\gamma = \eta_2(H)\rho^{\eta_1(H)}, \quad (11)$$

where η_1 and η_2 are both functions of the Hurst exponent H. Figure 5 presents the dependence of η_1 and η_2 on the Hurst exponent H, indicating that η_1 increases linearly with increasing H, with the opposite trends for η_2. Thus, overall,

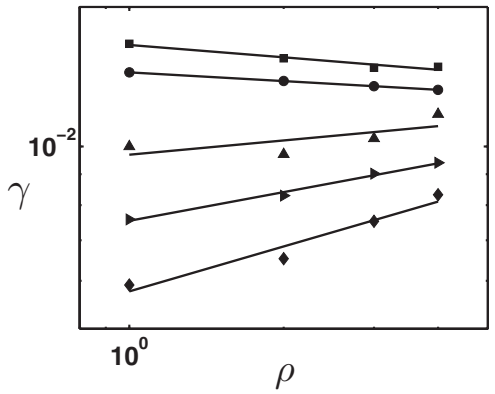

FIG. 4. The coefficient γ versus fracture density ρ for the Hurst exponents $H = 0.25$ (■), 0.3 (●), 0.5 (▲), 0.6 (▶), and 0.75 (♦).

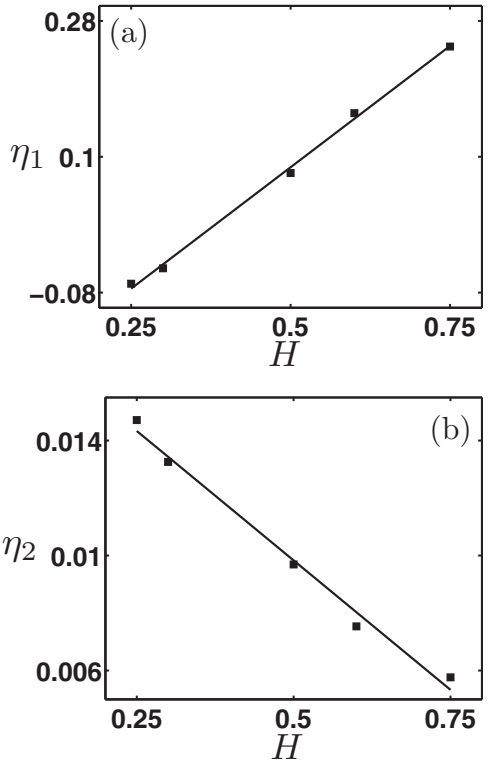

FIG. 5. (a) η_1 and (b) η_2 [see Eq. (11)] versus the Hurst exponent H.

we write

$$A \propto \exp[-(-c_1 H + c_2)\rho^{c_3 H - c_4} x]. \tag{12}$$

A fit of the numerical data yielded, $c_1 = c_2 \approx 0.02$, $c_3 \approx 0.64$, and $c_4 \approx 0.24$. Similar relations were obtained for the decay of the amplitude A at large distances x from the source. Thus, we write

$$A \propto \exp[-\beta(\rho, H)x] \tag{13}$$

with

$$\beta = \varepsilon_2(H)\rho^{\varepsilon_1(H)}. \tag{14}$$

Figure 6 presents the coefficient β as a function of the fracture number density ρ and Hurst exponent H, in the limit of large distances from the source. For a fixed H, the dependence of β on ρ is weak. The reason is that at large distances x from the source, the waves have already sampled the structure of the fracture network, and, therefore, it is unlikely that they encounter any new type of local structure of the network that they have not "seen" before.

On the other hand, the dependence of ε_1 and ε_2 on the Hurst exponent H is relatively strong and is similar to that of η_1 and η_2; this is shown in Fig. 7. The reason is twofold. One is that varying H produces a wide variety of heterogeneous matrix, particularly if $H < 0.5$. The second reason is linked with the nature of the FBM. Self-affine stochastic distributions, such as the FBM, are *not self-averaging*. Recall that the correlation length of the FBM is infinite, as large as the size of the system. That means that as the length scale of observations increases from small to large, no scale is reached beyond which the

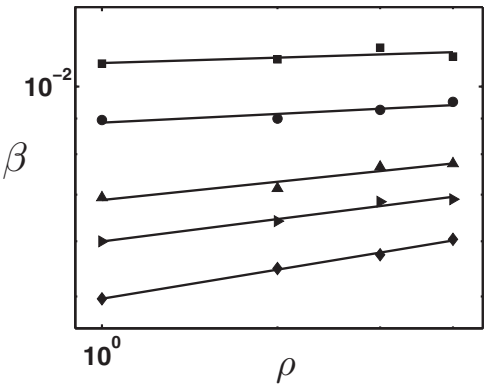

FIG. 6. The coefficient β as a function of fracture density ρ for the Hurst exponents $H = 0.25$ (■), 0.3 (●), 0.5 (▲), 0.6 (►), and 0.75 (♦).

behavior of the system is independent of the length scale. Thus, as the waves sample the porous medium at larger scales, they still "see" features in the distribution of the bulk modulus that they had not seen at smaller scales. Thus, we write

$$A \propto \exp[-(-c_5 H + c_6)\rho^{c_7 H - c_8} x] \tag{15}$$

with $c_5 = c_6 \approx 0.01$, $c_7 \approx 0.22$, and $c_8 \approx 0.03$, computed by fitting the numerical results.

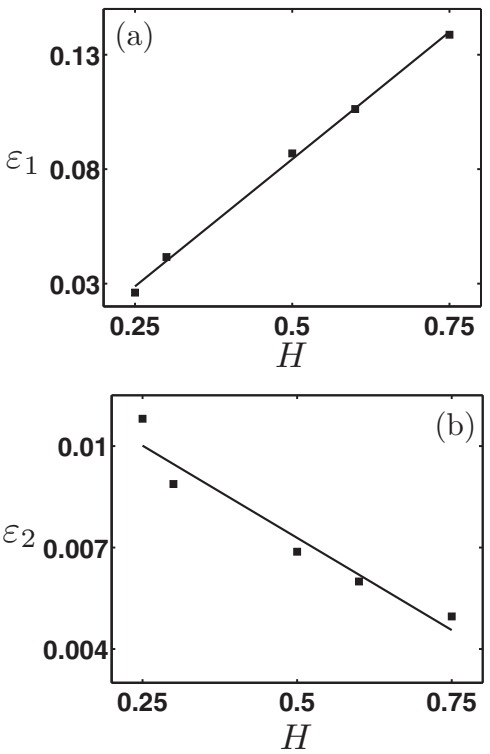

FIG. 7. The exponent (a) ε_1 and coefficient (b) ε_2 [see Eq. (14)] versus the Hurst exponent H.

B. The localization length

Given Eq. (15), it is then clear that the localization length ξ is given by

$$\xi \propto \beta(\rho, H)^{-1} \tag{16}$$

and therefore

$$\xi \propto \frac{1}{f_1(H)} \frac{1}{\rho^{f_2(H)}} \tag{17}$$

with the two functions $f_1(H)$ and $f_2(H)$ given by Eq. (15) as the inverse of the prefactor and the power of fracture density ρ.

In the geophysics literature on wave propagation in porous and fractured media no attention has been paid to the localization length, whereas, as mentioned earlier, ξ sets the distance beyond which any receiver of the waves scattered by the media will not record useful information and what it receives represents only statistical noise. Equation (17) indicates that the localization length is a strong function of both the correlations in the spatial distribution of the bulk modulus and the fracture density. This is, in our opinion, an important result.

C. The waves' energy

Figure 8 presents the decay of the energy of the pulse as a function of the distance x from the source, indicating that E_P decays exponentially with x for both short and large

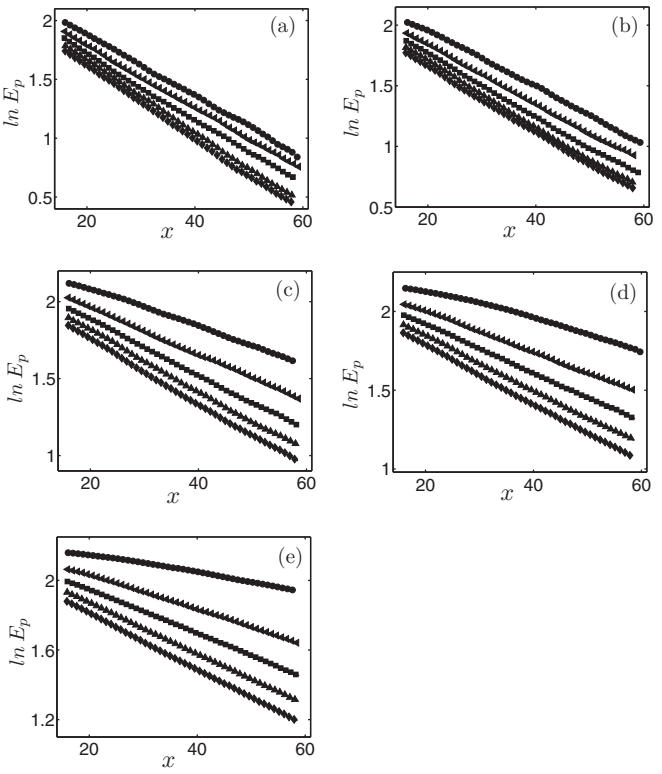

FIG. 8. Decay of the energy E_P versus distance x from the source for the Hurst exponents (a) $H = 0.25$, (b) 0.3, (c) 0.5, (d) 0.6, and (e) 0.75. The data are for fracture densities $\rho = 0$ (●), 1 (◀), 2 (■), 3 (▲), and 4 (♦).

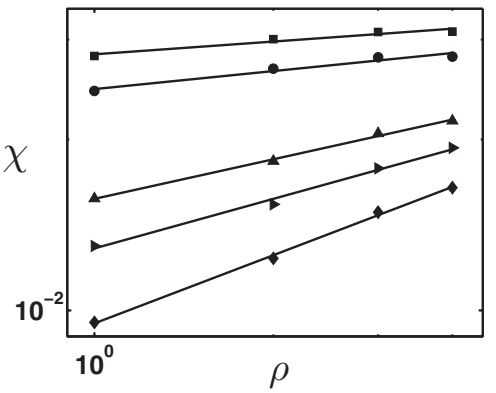

FIG. 9. The coefficient χ as a function of the fracture density ρ for the Hurst exponent $H = 0.25$ (■), 0.3 (●), 0.5 (▲), 0.6 (▶), and 0.75 (♦).

distances from the source, whereas E_p decays with x as a stretched exponential function when the matrix is uniform [30]. Therefore,

$$E_P \propto \exp[-\chi(\rho, H)x]. \tag{18}$$

Figure 9 displays the coefficient χ versus ρ for various Hurst exponents H, according to which χ also varies as a power law with the fracture density,

$$\chi = \mu_2(H)\rho^{\mu_1(H)}. \tag{19}$$

As shown in Fig. 10, μ_1 and μ_2 both depend linearly on the Hurst exponent H. Thus, similar to the amplitude A, for

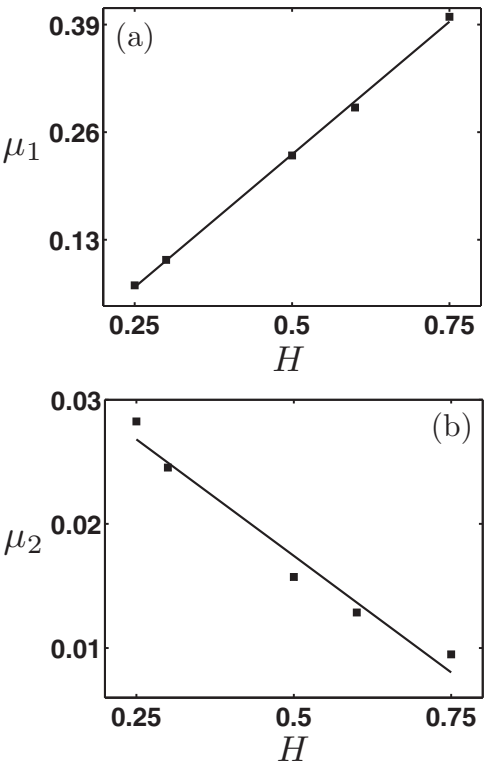

FIG. 10. (a) μ_1 and (b) μ_2 [see Eq. (19)] versus the Hurst exponent H.

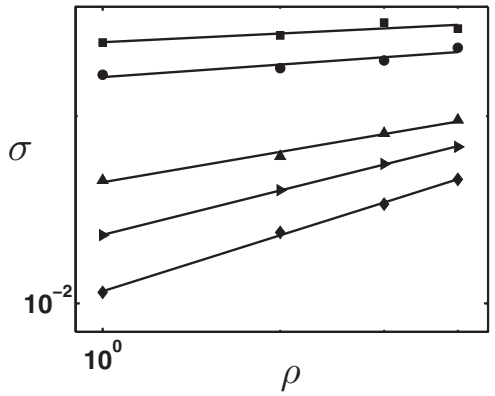

FIG. 11. The coefficient σ versus fracture density ρ for the Hurst exponents $H = 0.25$ (■), 0.3 (●), 0.5 (▲), 0.6 (►), and 0.75 (♦).

small x,

$$E_P \propto \exp[-(-a_1 H + a_2)\rho^{a_3 H - a_4} x], \tag{20}$$

with $a_1 = a_2 \approx 0.04$, $a_3 \approx 0.64$, and $a_4 \approx 0.09$. At large distances x from the source E_p still decays exponentially with x, but with different slope. So

$$E_P \propto \exp[-\sigma(\rho, H)x] \tag{21}$$

with

$$\sigma = \nu_2(H)\rho^{\nu_1(H)}. \tag{22}$$

In Fig. 11 we plot the coefficient σ as a function of ρ. Once again, as shown in Fig. 12, both ν_1 and ν_2 vary linearly with

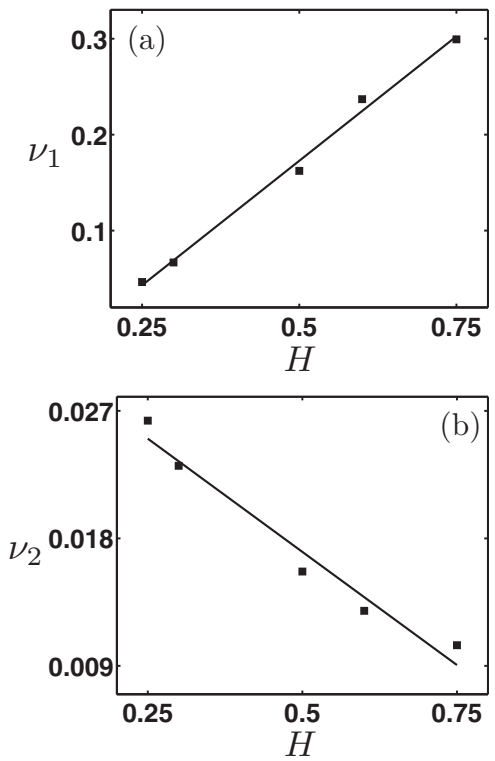

FIG. 12. (a) ν_1 and (b) ν_2 [see Eq. (22)] versus the Hurst exponent H.

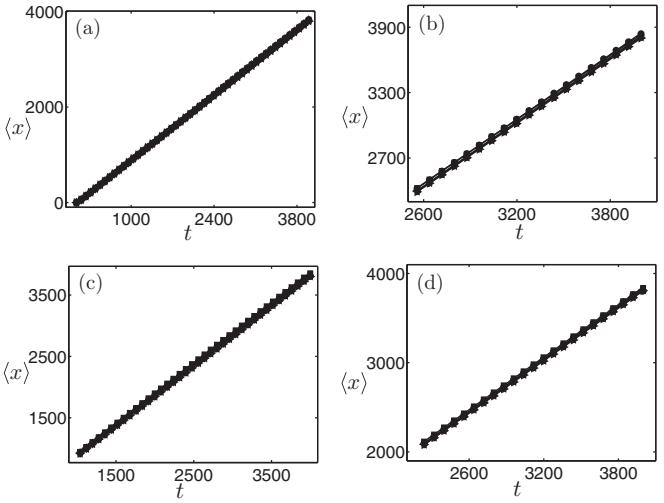

FIG. 13. Mean traveled distance $\langle x \rangle$ versus time t for the Hurst exponents (a) $H = 0.25$, (b) 0.5, (c) 0.6 and (d) 0.75. The data are for the fracture number densities $\rho = 0$ (■), 1 (●), 2 (♦), 3 (◄), and 4 (►).

H. Thus, at large distances x from the source,

$$E_P \propto \exp[-(-a_5 H + a_6)\rho^{a_7 H - a_8} x], \tag{23}$$

with $a_5 = a_6 \approx 0.03$, $a_7 \approx 0.52$ and $a_8 \approx 0.09$. Note that in all the cases, Eqs. (12), (15), (20), and (23), the coefficients c_i and a_i in the linear prefactor are small.

D. Mean speed of wave propagation and its dependence on orientation

The mean speed of wave propagation provides clues to the structure of a porous formation. In Fig. 13 we plot the mean distance $\langle x \rangle$ of the wave front in the main direction of propagation as a function of time and present its dependence on the fractures' number density ρ and the Hurst exponent H. Surprisingly, the dependence of $\langle x \rangle$ on both ρ and H is very weak, for which we have no reasonable explanation. The slopes of the results shown in Fig. 13 represent the mean speeds v of propagation of the acoustic waves. Thus, given that $\langle x \rangle$ is practically independent of fracture density and the Hurst exponent, the mean speed v of propagation is practically constant and independent of both parameters. We do not, however, expect this to be true if a fractured porous medium contains fluids, and in particular when the fracture network forms a sample-spanning cluster across the medium through which fluids flow.

The mean wave speed v does, however, depend on the mean orientation of the fractures. Thus, we carried out a series of simulations in which we varied the mean orientation of the fractures. Figure 14 presents five cases that we studied. The orientations of the fractures were assumed to follow a Gaussian distribution in which the mean orientations for the five cases of Fig. 14 were 0, $\pi/6$, $\pi/4$,$\pi/3$, and $\pi/2$, while the standard deviations of the distribution was held fixed. These fracture networks are, of course, anisotropic. Figure 15 presents the results. We find that under these condition,

$$v = v_0 - 0.0012\rho\theta, \tag{24}$$

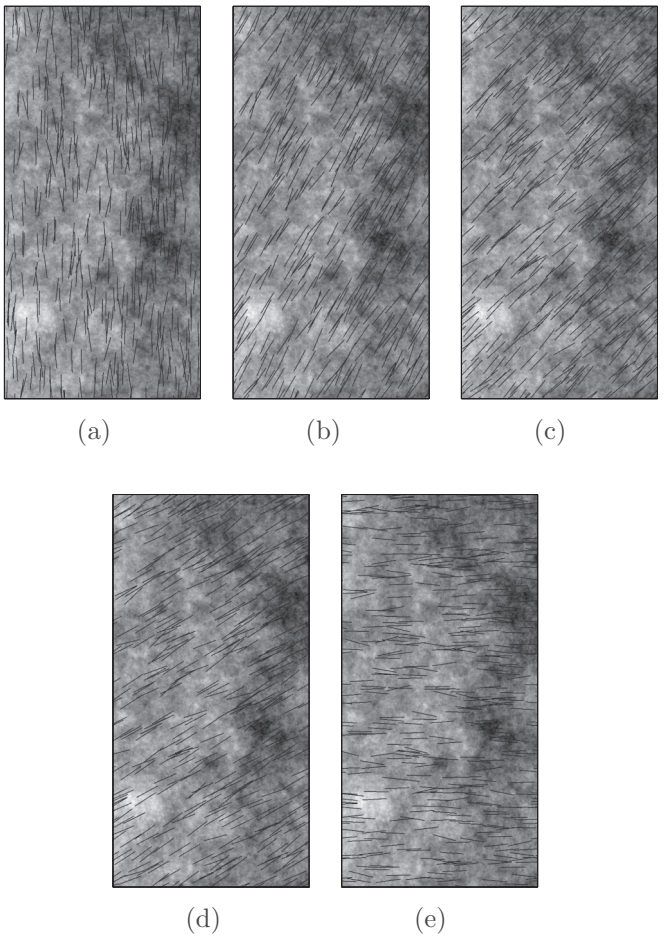

FIG. 14. Five models of fractured porous media in which the mean orientation of the fractures is (a) 0; (b) $\pi/6$; (c) $\pi/4$; (d) $\pi/3$, and (e) $\pi/2$. Lighter colors indicate larger bulk modulus.

where θ is the mean orientation of the fractures, and v_0 is the wave speed for $\theta = 0$. The linear dependence of v on the mean orientation of the fractures agrees with the theoretical predictions of Chapman [58].

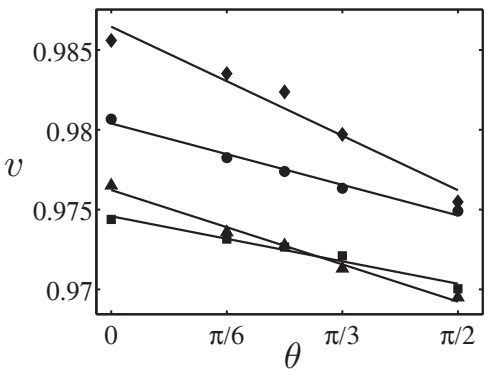

FIG. 15. Dependence of the mean speed on the fracture density and mean orientation of the fractures.

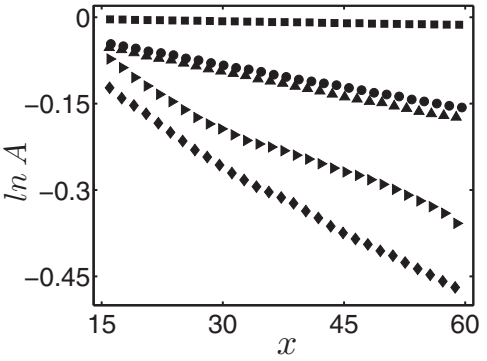

FIG. 16. Comparison of the decay of the wave amplitude A in various types of the unfractured and fractured porous media in which the bulk modulus of the porous matrix follows a white noise without a fracture network (■), a uniform distribution with a fracture network (●), a white noise with a fracture network (▲), a FBM distribution without a fracture network (►), and a FBM distribution with a fracture network (♦). The fractures' number density ρ and the Hurst exponent H are 2 and 0.5, respectively.

E. Comparison of unfractured and fractured porous media

As pointed out in the introduction, one main goal of this paper is to compare wave propagation in unfractured and fractured porous media. Hence, we compare in Fig. 16 the decay of the amplitude A with the distance x from the source. Shown are the results for two fractured and two unfractured porous media and with heterogeneous and uniform matrices. As can be seen, the decay of the amplitude is a strong function of the heterogeneity of porous media, and in particular their fracture network and spatial distribution of their bulk modulus.

VI. SUMMARY

The main goal of this paper was to compare wave propagation in fractured porous media with a uniform matrix with one in which, in accordance with the experimental data [8], the bulk modulus is spatially distributed according to a fractional Brownian motion. We presented numerical results that indicated that the waves' amplitude decays exponentially fast with the distance x from the source for all values of x, when the bulk modulus in the matrix is distributed according to a FBM. This is in sharp contrast with the case [30] in which the matrix is uniform and not only does the amplitude decay with the distance as a stretched exponential function, but the exponent that characterizes the function is dependent upon the fracture density.

The comparison is important from a practical view point. First, in the traditional models of fractured rock, particularly when they are used to study wave propagation or fit some data, the matrix is assumed to be uniform. But, as our results indicate, there are fundamental differences between models in which the matrix is uniform and those in which the matrix is heterogeneous and its properties are spatially distributed according to self-affine distributions. Second, that the wave amplitude decays exponentially fast with the distance from the source when the matrix is heterogeneous may be considered as a signature of highly heterogeneous fractured porous media and perhaps be used as a sort of diagnostic tool.

[1] P. M. Adler and J.-F. Thovert, *Fractures and Fracture Networks* (Kluwer, Dordrecht, 1999).

[2] M. Sahimi, *Flow and Transport in Porous Media and Fractured Rock*, 2nd ed. (Wiley-VCH, Weinheim, 2011); Rev. Mod. Phys. **65**, 1393 (1993).

[3] P. M. Adler, J.-F. Thovert, and V. V. Mourzenko, *Fractured Porous Media* (Oxford University Press, Oxford, 2013).

[4] T. A. Hewett, Fractal distributions of reservoir heterogeneity and their influence on fluid transport, SPE paper 15386 (1986); https://www.onepetro.org/conference-paper/SPE-15386-MS.

[5] B. B. Mandelbrot and J. W. van Ness, Fractional Gaussian motion, fractional Gaussian noise and their applications, SIAM Rev. **10**, 422 (1968).

[6] S. P. Neuman, Generalized scaling of permeabilities: Validation and the effect of support scale, Geophys. Res. Lett. **21**, 349 (1994).

[7] S. Mukhopadhyay and M. Sahimi, Calculation of the effective permeabilities of field-scale porous media, Chem. Eng. Sci. **55**, 4495 (2000).

[8] M. Sahimi and S. E. Tajer, Self-affine distributions of the bulk density, elastic moduli, and seismic wave velocities of rock, Phys. Rev. E **71**, 046301 (2005).

[9] C. C. Barton and E. Larsen, in *Proceedings of the International Symposium on Fundamentals of Rock Joints*, edited by O. Stephansson (Bjorkliden, Sweden, 1985), p. 77.

[10] P. LaPointe, A method to characterize fracture density and connectivity through fractal geometry, Int. J. Rock Mech. Min. **25**, 421 (1988).

[11] E. Bonnet, O. Bour, N. E. Odling, P. Davy, I. Main, P. Cowie, and B. Berkowitz, Scaling of fracture systems in geological media, Rev. Geophys. **39**, 347 (2001).

[12] A. B. Kersting, D. W. Efurd, D. L. Finnegan, D. J. Rokop, D. K. Smith, and J. L. Thompson, Migration of plutonium in ground water at the Nevada test site, Nature (London) **397**, 56 (1999).

[13] T. L. Chelidze, Percolation and fracture, Phys. Earth Planet. Int. **28**, 93 (1982).

[14] S. R. Brown, C. H. Scholz, and J. B. Rundle, A simplified spring-block model of earthquakes, Geophys. Res. Lett. **18**, 215 (1991).

[15] C. G. Bufe, S. P. Nishenko, and D. J. Varnes, Seismicity trends and potential for large earthquakes in the Alaska-Aleutian region, Pure Appl. Geophys. **142**, 83 (1994).

[16] M. Sahimi, M. C. Robertson, and C. G. Sammis, Fractal Distribution of Earthquake Hypocenters and its Relation with Fault Patterns and Percolation, Phys. Rev. Lett. **70**, 2186 (1993).

[17] M. C. Robertson, C. G. Sammis, M. Sahimi, and A. J. Martin, Fractal analysis of three-dimensional spatial distribution of earthquakes with a percolation interpretation, J. Geophys. Res. B **100**, 609 (1995).

[18] D. Pastén, M. Muñoz, A. Armando, J. Rogan, and J. A. Valdivia, Monofractal and multifractal analysis of the spatial distribution of earthquakes in the central zone of Chile, Phys. Rev. E **84**, 066123 (2011).

[19] T. A. Tafti, M. Sahimi, F. Aminzadeh, and C. G. Sammis, Use of microseismicity for determining the structure of the fracture network of large-scale porous media, Phys. Rev. E **87**, 032152 (2013).

[20] H. Dashtian, G. R. Jafari, M. Sahimi, and M. Masihi, Scaling, multifractality, and long-range correlations in well log data of large-scale porous media, Physica A **390**, 2096 (2011).

[21] H. Dashtian, G. R. Jafari, Z. Koohi Lai, M. Masihi, and M. Sahimi, Analysis of cross correlations between well logs of hydrocarbon reservoirs, Transp. Porous Media **90**, 445 (2011).

[22] H. Dashtian, Y. Yang, and M. Sahimi, Non-universality of the Archie exponent due to multifractality of the resistivity well logs, Geophys. Res. Lett. **42**, 10655 (2015).

[23] A. Ishimaru, *Wave Propagation and Scattering in Random Media* (Academic, New York, 1978).

[24] N. Bleistein, J. K. Cohen, and J. W. Stockwell, Jr., *Mathematics of Multidimensional Seismic Imaging, Migration, and Inversion* (Springer, New York, 2001).

[25] F. Shahbazi, A. Bahraminasab, S. M. Vaez Allaei, M. Sahimi, and M. R. Rahimi Tabar, Localization of Elastic Waves in Heterogeneous Media with Off-Diagonal Disorder and Long-Range Correlations, Phys. Rev. Lett. **94**, 165505 (2005).

[26] A. Bahraminasab, S. M. Vaez Allaei, F. Shahbazi, M. Sahimi, M. D. Niry, and M. R. Rahimi Tabar, Renormalization group analysis and numerical simulation of propagation and localization of acoustic waves in heterogeneous media, Phys. Rev. B **75**, 064301 (2007).

[27] R. Sepehrinia, A. Bahraminasab, M. Sahimi, and M. R. Rahimi Tabar, Dynamic renormalization group analysis of propagation of elastic waves in two-dimensional heterogeneous media, Phys. Rev. B **77**, 014203 (2008).

[28] R. Sepehrinia, M. R. Rahimi Tabar, and M. Sahimi, Numerical simulation of localization of elastic waves in two- and three-dimensional heterogeneous media, Phys. Rev. B **78**, 024207 (2008).

[29] S. M. Vaez Allaei and M. Sahimi, Shape of a Wave Front in a Heterogeneous Medium, Phys. Rev. Lett. **96**, 075507 (2006).

[30] H. Hamzehpour, F. H. Kasani, M. Sahimi, and R. Sepehrinia, Wave propagation in disordered fractured porous media, Phys. Rev. E **89**, 023301 (2014).

[31] A. Yazdi, H. Hamzehpour, and M. Sahimi, Permeability, porosity, and percolation properties of two-dimensional disordered fracture networks, Phys. Rev. E **84**, 046317 (2011).

[32] H. Hamzehpour, A. Atakhani, A. K. Gupta, and M. Sahimi, Electro-osmotic flow in disordered porous and fractured media, Phys. Rev. E **89**, 033007 (2014).

[33] H. Hamzehpour, V. V. Mourzenko, J.-F. Thovert, and P. M. Adler, Percolation and permeability of networks of heterogeneous fractures, Phys. Rev. E **79**, 036302 (2009).

[34] M. Khoshhali and H. Hamzehpour, Wave front properties of acoustic wave in disorder fractured media, Transp. Porous Media **107**, 129 (2015).

[35] J. Garnier and K. Sølna, Effective fractional acoustic wave equations in random multiscale media, J. Acoust. Soc. Am. **127**, 62 (2010).

[36] I. A. Beresnev and P. A. Johnson, Elastic-wave stimulation of oil production: A review of methods and results, Geophysics **59**, 1000 (1994).

[37] D. R. Schmitt, Seismic attributes for monitoring of a shallow heated heavy oil reservoir: A case study, Geophysics **62**, 368 (1999).

[38] J. I. G. Cidoncha, *Application of Acoustic Waves for Reservoir Stimulation*, SPE Paper 108643 (Society of Petroleum Enginers, Richardson, Texas, 2007).

[39] Y. Liu, Acoustic properties of reservoir fluids, Ph.D. thesis, Stanford University, 1998.

[40] S. Sinanovic, D. H. Johnson, V. V. Shah, and W. R. Gardner, Data communication along the drill string using acoustic waves, in *Proceedings of Acoustics, Speech, and Signal Processing* (IEEE, Montreal, Quebec, Canada, 2004), Vol. 4, pp. 909–912.

[41] J. B. U. Haldorsen, D. L. Johnson, T. Plona, B. Sinha, H.-P. Valero, and K. Winkler, Borehole acoustic waves, Oilfield Rev., Spring (Schlumberger, USA, 2006); http://www.slb.com/resources/oilfield_review/en/2006/or2006_spr.aspx.

[42] M. Sahimi and M. Hashemi, Wavelet identification of the spatial distribution of fractures, Geophys. Res. Lett. **28**, 611 (2001).

[43] E. L. Hardin, C. H. Cheng, F. L. Paillet, and J. D. Mendelson, Fracture characterization by means of attenuation and generation of tube waves in fractured crystalline rock at Mirror Lake, New Hampshire, J. Geophys. Res: Solid Earth **92**, 7989 (1987).

[44] E. H. Saenger, N. Gold, and S. A. Shapiro, Modeling the propagation of elastic waves using a modified finite-difference grid, Wave Motion **31**, 77 (2000).

[45] E. H. Saenger and S. A. Shapiro, Effective velocities in fractured media: A numerical study using the rotated staggered finite-difference grid, Geophys. Prospect. **50**, 183 (2002).

[46] E. H. Saenger, O. S. Krüger, and S. A. Shapiro, Effective elastic properties of randomly fractured soils: 3D numerical experiments, Geophys. Prospect. **52**, 183 (2004).

[47] E. Charlaix, Percolation threshold of a random array of discs: A numerical simulation, J. Phys. A **18**, L533 (1986).

[48] R. J. O'Connell and B. Budiansky, Seismic velocities in dry and saturated cracked solids, J. Geophys. Res. **79**, 5412 (1974).

[49] B. Orlowsky, E. H. Saenger, Y. Guǵuen, and S. A. Shapiro, Effect of parallel crack distributions on effective elastic properties: A numerical study, Int. J. Fracture **124**, L171 (2003).

[50] S. Vlastos, E. Liu, I. G. Main, and X.-Y. Li, Numerical simulation of wave propagation in media with discrete distributions of fractures: Effects of fracture sizes and spatial distributions, Geophys. J. Int. **152**, 649 (2003).

[51] S. Vlastos, E. Liu, I. G. Main, M. Schoenberg, C. Narteau, X. Y. Li, and B. Maillot, Dual simulations of fluid flow and seismic wave propagation in a fractured network: Effects of pore pressure on seismic signature, Geophys. J. Int. **166**, 825 (2006).

[52] C. Narteau, Formation and evolution of a population of strike-slip faults in a multiscale cellular automaton model, Geophys. J. Int. **168**, 723 (2007).

[53] F. Hall and Y. Wang, Elastic wave modeling by an integrated finite difference method, Geophys. J. Int. **177**, 104 (2009).

[54] A. L. Fetter and J. D. Walecka, *Theoretical Mechanics of Particles and Continua*, 2nd ed. (Dover, New York, 2003).

[55] K. R. Symon, *Mechanics*, 2nd ed. (Addison-Wesley, Reading, 1960), p. 295.

[56] M. A. Dablain, The application of high-order differencing to the scalar wave equation, Geophysics **51**, 54 (1986).

[57] G. Kneib and C. Kerner, Accurate and efficient seismic modeling in random media, Geophysics **58**, 576 (1993).

[58] M. Chapman, Frequency-dependent anisotropy due to meso-scale fractures in the presence of equant porosity, Geophys. Prospect. **51**, 369 (2003).